Received: 13 December 2022 | Revised: 6 March 2023 | Accepted: 13 March 2023

DOI: 10.1002/cm.21753

RESEARCH ARTICLE

CYTOSKELETON WILEY

CD109-regulated mechanical properties of endothelial cells

Maria N. Starodubtseva[1,2] | Ju Liu[3] | Eldar A. Nadyrov[1] | Nastassia M. Shkliarava[2] | Alena U. Sadouskaya[2] | Ivan E. Starodubtsev[4] | Sergey L. Achinovich[5] | Xianli Meng[6] | Dmitry A. Zinovkin[1] | Md Zahidul Islam Pranjol[7]

[1]Gomel State Medical University, 5 Lange str, Gomel BY-246000, Belarus

[2]Institute of Radiobiology of NAS of Belarus, 4 Fedyuninskogo str, Gomel BY-246007, Belarus

[3]Shandong Provincial Qianfoshan Hospital, Shandong University, Jinan, Shandong, 250014, People's Republic of China

[4]Belarusian State University, 4 Nezavisimosti av, Minsk BY-220030, Belarus

[5]Gomel Clinical Oncology Center, 2 Meditsinskaya str, Gomel BY-246041, Belarus

[6]School of Pharmacy, Shandong First Medical University, Jinan, Shandong, 250014, People's Republic of China

[7]Department of Biochemistry, School of Life Sciences, University of Sussex, Brighton BN1 9QG, UK

Correspondence
Md Zahidul Islam Pranjol, Department of Biochemistry, School of Life Sciences, University of Sussex, Brighton, UK.
Email: z.pranjol@sussex.ac.uk

Funding information
Belarusian Republican Foundation for Fundamental Research; National Natural Science Foundation of China

Abstract

CD109 antigen on the endothelial cell surface plays an important role in vascular pathology. The aim of the work was to investigate the effect of the immobilization of CD109 antigen with specific antibodies on nanomechanical properties of human umbilical endothelial cells (HUVECs) using atomic force microscopy in quantitative nanomechanical property mapping mode (PeakForce QNM). Anti-CD109 antibodies induced significant stiffening of the cell surface Me(LQ; UQ): in 1.45(1.07;2.29) times with respect to control cells for fixed cells and in 4.9(3.6;5.9) times with respect to control cells for living cells, and changes in the spatial distribution of cell surface mechanical properties. The changes in the HUVEC's mechanical properties were accompanied by the activation of the TGF-/Smad2/3 signaling pathway and reorganization of the vimentin and actin cytoskeletal elements. Our findings show that blocking CD109 antigen using anti-CD109 antibodies leads in HUVECs to the processes similar to that occur after cell TGF-β-signaling activation. Therefore, we suggest that CD109 antigen may be involved in regulating the mechanical behavior of endothelial cells.

KEYWORDS
adhesion force, atomic force microscopy, CD109, endothelial cell, PeakForce QNM, stiffness, TGF-β signaling

1 | INTRODUCTION

CD109 is a glycosylphosphatidylinositol (GPI)-anchored glycoprotein and a member of the α2-macroglobulin/C3, C4, C5 family of thioester-containing proteins (Lin et al., 2002). CD109 is a potential regulator of many signaling pathways including TGF-β (Luckstadt et al., 2021), YAP/TAZ (Minata et al., 2019), EGFR/AKT/mTOR (Lee et al., 2020), EGFR and STAT3 signaling (Mo et al., 2020). In endothelial cells, CD109 plays an important role in various pathologies (Mii et al., 2019). For instance, CD109 acts as a marker for circulating endothelial cells in glioblastoma (Cuppini et al., 2013). Additionally, this glycoprotein is a TGF-β co-receptor and a potent inhibitor of the TGF-β signaling that induces and promotes tumor cell migration and invasion (Zhou, Cecere, & Philip, 2017). The expression levels of CD109 have been recently shown in cultured squamous cell carcinoma cells to inversely correlate with the level of the activation of

Abbreviations: ABs, antibodies; AFM, atomic force microscopy; DMT Modulus, elastic modulus measured using Derjaguin–Muller–Toporov model; HUVECs, human umbilical vein endothelial cells; IgG, immunoglobulin G; QNM, quantitative nanomechanical mapping; TGF-β, transforming growth factor beta.

TGF-β signaling, epithelial-to-mesenchymal transition, migration, and invasion, suggesting a role of CD109 as a gatekeeper of the epithelial phenotype by regulating the TGF-β pathway (Zhou, da Silva, Siegel, & Philip, 2019). CD109 protein binds directly with TGF-β1 forming complexes with the signaling receptor kinases. This binding relates to the process of receptor internalization and degradation (Tzavlaki & Moustakas, 2020).

Among others, TGF-β has been shown to induce cardiac fibrosis, which leads to increased myocardial stiffness and, ultimately, to cardiac dysfunction and heart failure (Souders, Borg, Banerjee, & Baudino, 2012; Sullivan & Black, 2013). For example, the expression of TGF-β1 increases with the development of cardiac hypertrophy (Ruwhof, 2000), dilated cardiomyopathy (Khan & Sheppard, 2006) and aortic stenosis (Beaumont et al., 2014), and crucially, myocardial infarction (de Sousa Lopes et al., 2003; Frantz et al., 2008). In atherosclerosis, the fibrous and inflammatory components of the lesion in the vessel wall is mostly likely modulated by TGF-β. For instance, an increased expression of TGF-β1 in atherosclerotic plaques has been shown to correlate with progressive atherosclerosis patients (Herder et al., 2012; Panutsopulos et al., 2005).

Endothelial cells lining the interior of blood and lymph vessels can undergo a transition to mesenchymal cells, a process known as endothelial-to-mesenchymal transition (Kovacic, Mercader, Torres, Boehm, & Fuster, 2012). Concomitant loss of functional endothelial cells could also lead to a decrease in capillary density, thus causing tissue ischemia, which is a potent factor in the fibrous process (Kruithof, Duim, Moerkamp, & Goumans, 2012).

In the present work, to test the hypothesis that a CD109 antigen can be involved into the regulation of the mechanical behavior of endothelial cells we use specific antibodies (ABs) against CD109 antigen for immobilization of the antigen and blocking its ability to downregulate TGF-β signaling in endothelial cells using the human umbilical vein endothelial cells (HUVECs) as a cell model. We examine CD109-dependent changes of the nanomechanical properties of cell surface and cytoskeleton remodeling in HUVECs.

2 | RESULTS

2.1 | Effect of anti-CD109 antibodies on the morphology and cytoskeleton of HUVECs

CD109 is known to be a negative regulator of the TGF-β pathways that activate the endothelial-to-mesenchymal transition with cytoskeleton rearrangement and cell morphology change. Anti-CD109 ABs have, in addition to specific CD109 binding sites on Fab fragments, Fc fragments that bind to Fc receptors on the cell surface, which can blur or even mask the effects of specific interactions of endothelial cells with anti-CD109 ABs. Fc receptors are known to be expressed by endothelial cells in various organs (Roopenian & Akilesh, 2007). FcRn (the neonatal Fc receptor) participates in the transport of IgG produced by HUVECs into the umbilical vein and arteries (Zhao, Liu, Chen, Korteweg, & Gu, 2011). Therefore, to eliminate the specific CD109-associated effect, firstly, it was necessary to block Fc receptors with IgG. To block the nonspecific interaction of ABs with cellular Fc receptors of the HUVEC surface, we used IgG following a protocol from R&D systems (https://www.rndsystems.com/resources/protocols). The study of the expression of SMAD proteins of the classical mechanism of TGF-β signaling showed an overexpression of SMAD2 and SMAD3 proteins in HUVECs after exposure of IgG-pretreated cells to anti-CD109 ABs (Figure A in Appendix S1), which indicated the activation of SMAD2/3 signaling pathways in HUVECs using anti-CD109 ABs.

The changes in the cell morphology induced by treatment with IgG and anti-CD109 ABs were studied by both light microscopy (Figure 1a–c) and AFM (d–f) techniques. The interaction of HUVECs with IgG causes a decrease in the cell spreading area on slides (Figure 1j) and appearance and growth of filopodia (Figure 1h,k,l). After the subsequent cell treatment with anti-CD109 AB, the cell spreading area increased (Figure 2j) but no significant changes in the parameter related to filopodia formation were detected (Figure 1k,l).

The activation of TGF-β signaling pathways is known to lead to cytoskeleton remodeling with the intermediate filaments' reorganization (Gladilin et al., 2019; Melchionna, Trono, Tocci, & Nistico, 2021). Figure 2a–c represents the results of the immunocytochemical analysis of the vimentin cytoskeleton in the studied HUVEC's samples. Vimentin cytoskeletal structures were detected in anti-CD109 AB-treated cells in all cell zones but visually predominately in the perinuclear zone (Figure 3b,c). The percentage of vimentin structures increased by 1.5(1.1;2.0) times ($p < .0001$, Mann–Whitney U test) in HUVECs after the treatment with IgG and anti-CD109 ABs relative to control cells (Figure 2c).

3 | EFFECT OF ANTI-CD109 ANTIBODIES ON HUVEC'S MECHANICAL PROPERTIES

The reorganization of the cytoskeleton leads to a change in HUVEC's mechanical properties. The heterogeneity in the nanomechanical parameters of HUVECs has been recently demonstrated by the AFM technique (Starodubtseva et al., 2021). Three different zones of HUVECs, the nuclear, perinuclear, and peripheral zones had relatively different mechanical properties (Starodubtseva et al., 2021). Figure 3 presents the AFM images recorded on three channels (topography, DMT modulus, and adhesion) of the microscale areas of the fixed HUVEC's surface for three experimental samples (control cells, cells after IgG treatment, and cells after IgG + anti-CD109 AB treatment). The visual analysis of the images in Figure 3 reveals a difference in the spatial distribution of the parameters of elastic and adhesive properties of the HUVEC's surface for the studied sample.

The numerical analyses of the parameters of the structural properties of the cell surface for the studied samples showed that the roughness over the microscale areas of the cell surface increased significantly only after IgG treatment (Figure 4a) and within the nuclear cellular zone (all presented data in Figure 4b,c are not significant). Contrary to structural properties, a significant change in the

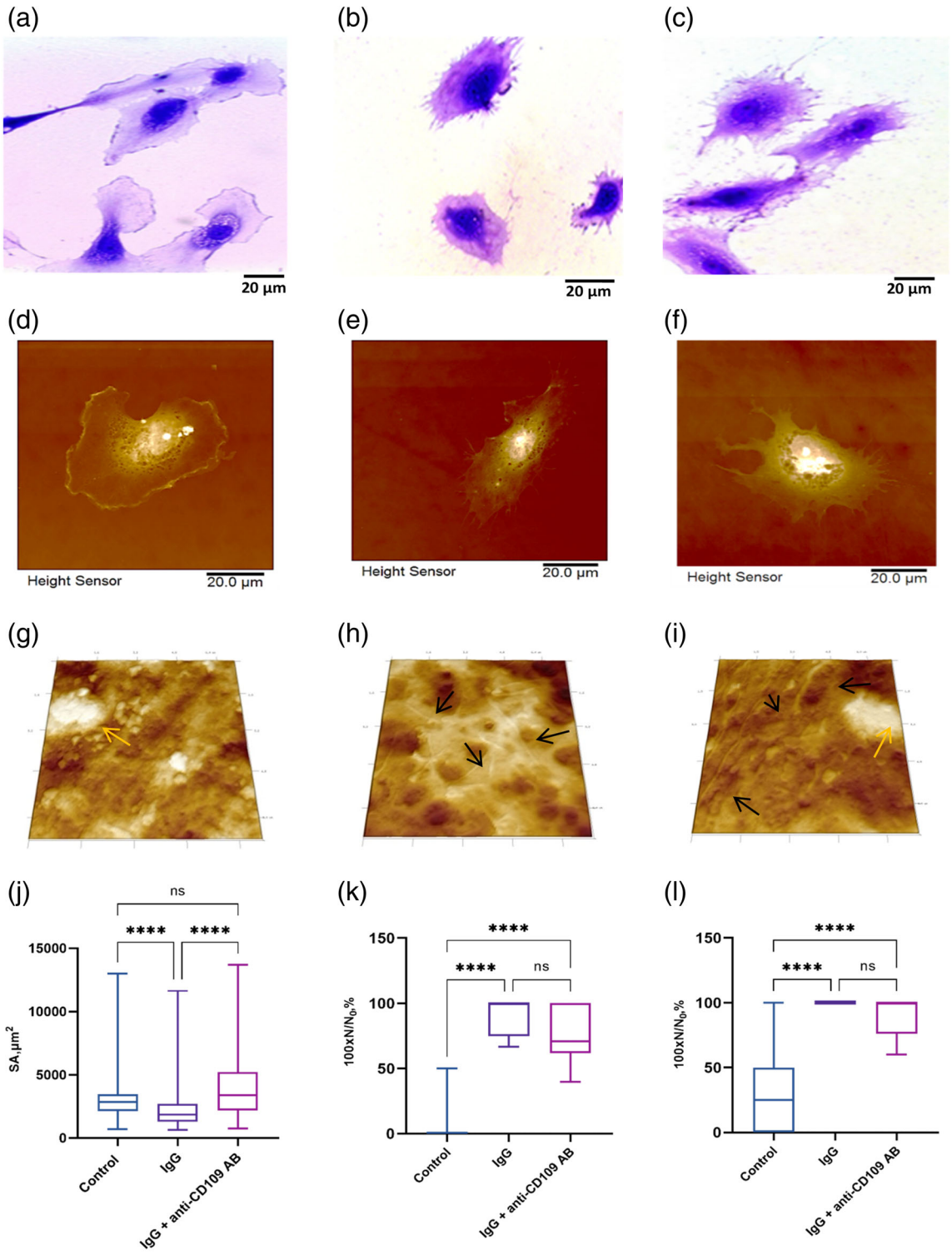

FIGURE 1 Effects of IgG and anti-CD109 ABs on HUVEC's morphology. (a–c) Light microscopy images of HUVECs: control (a), IgG-treated (b), IgG + anti-CD109 AB-treated cells (c). Cells were fixed with glutaraldehyde and dyed by Romanovsky-Giemsa. (d–f) AFM topographical images of HUVECs: control (d), IgG-treated (e), IgG + anti-CD109 AB-treated cells (f). Cells were fixed with glutaraldehyde. 256 × 256 pixels. (g–i) 3D AFM topographical images of the HUVEC surface for control (g), IgG-treated (h) and IgG + antiCD109 ABs-treated (i) cells. 7.0 µm × 7.0 µm. 256 × 256 pixels. The AFM images were recorded over a central cell zone. The black arrows point to filopodia, yellow arrows point to the nucleoli. (j–l) Morphological parameters of HUVECs: the cell spreading area (*SA*) (j), the percentage of cells (N/N_0) having filopodia protrusions at the leading edge (k) and on the cell body (l). *N* is a number of cells with filopodia in a corresponding area, N_0 is a total number of cells on light microscopy image. N_c is the median of the cell area stained in dark brown-violet color in cells of the control cell sample. Data are presented as median, interquartile interval limits (box), and maximal and minimal values (whiskers). Kruskal–Wallis test with Bonferroni correction: ****$p < .0001$; ns $p > .05$. $n = 100$ (j); $n = 16$ (k, l) for each group.

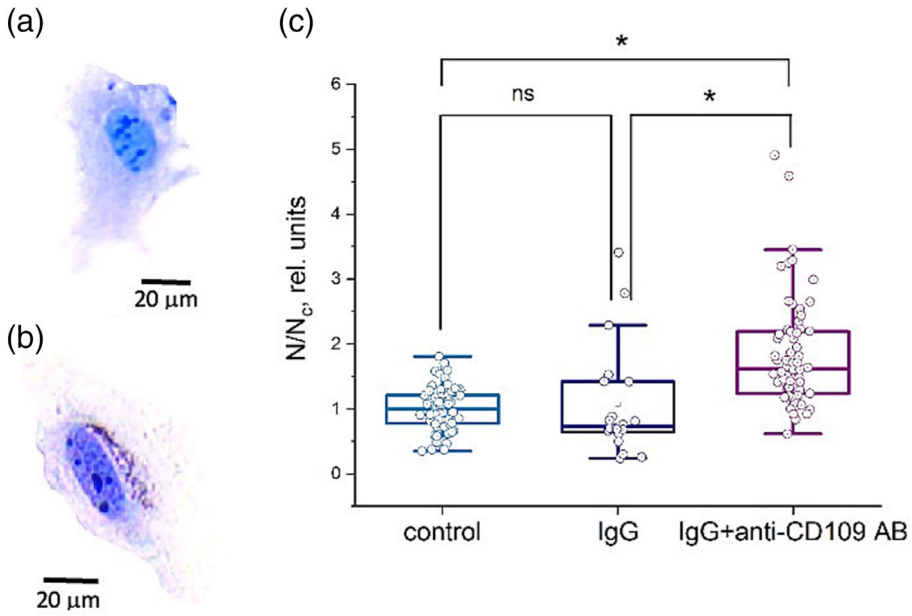

FIGURE 2 Effect of anti-CD109 antibodies on vimentin cytoskeleton in HUVECs. (a) The typical images of control HUVEC samples. (b) The typical images of anti-CD109 AB-treated HUVEC samples. Cells were treated with ABs, fixed with glutaraldehyde, stained by immunocytochemical method and then by Romanovsky-Giemsa as described in Materials and Methods. Vimentin cytoskeleton structures are visible in dark brown-violet color. (c) The relative content of vimentin in HUVEC samples relative to control ones (N/N_c). Parameter N/N_c in HUVEC samples was assessed relative to the control sample. N is the cell areas stained in dark brown-violet color (immunocytochemical staining against vimetin) for a studied cell sample. Data are presented as the median, interquartile interval limits (box), and maximal and minimal values (whiskers), experimental values (points). Kruskal–Wallis test with Bonferroni correction: * $p < .00001$; ns $p > .05$.

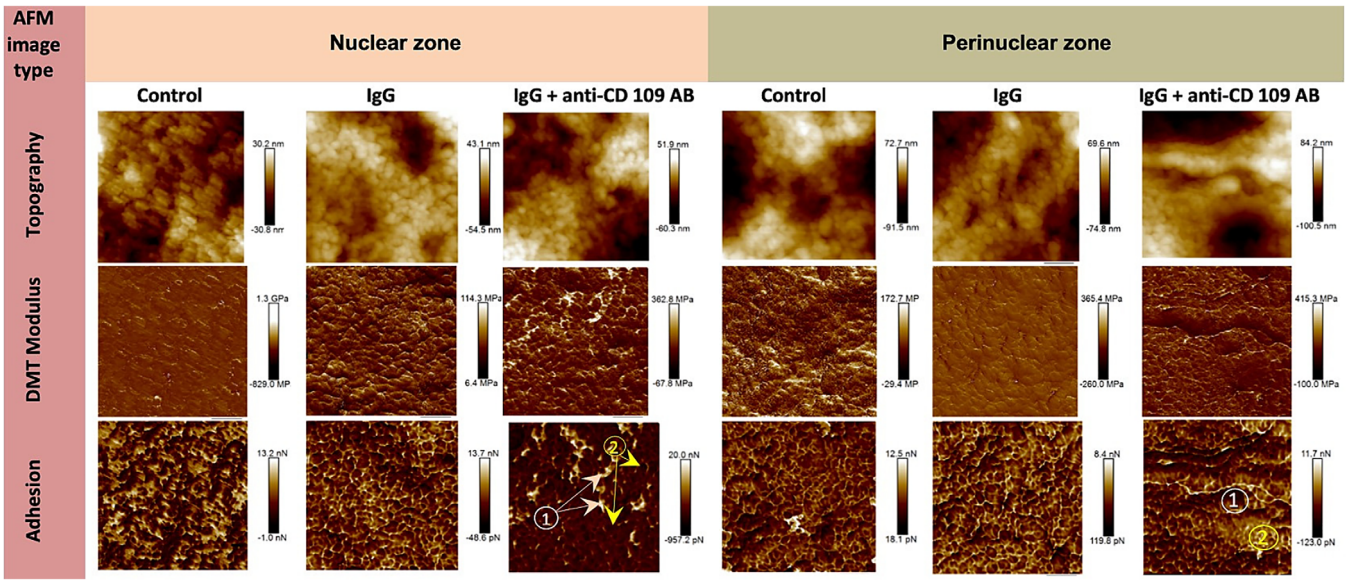

FIGURE 3 Typical AFM images of the microscale surface areas of control HUVECs, HUVECs after IgG treatment, and HUVECs after IgG + anti-CD109 AB treatment. The figure represents AFM images for two cell zones: nuclear (a) and perinuclear (b) zones. Peripheral cell zone is a thin layer consisting mainly the developed actin cytoskeleton network and the plasmalemma. Because the structural changes within the peripheral zone were insignificant, the AFM images for the peripheral zone were not presented. The scan sizes are 1 μm × 1 μm, resolution is 256 × 256 pixels. The adhesion maps clearly show spatially confined nanoscale regions with varying coloration grades for cell samples after IgG + anti-CD109 AB treatment (areas with lower adhesion are marked with number 1, and areas with higher adhesion are marked with number 2).

mechanical properties of the studied cells occurred when IgG-treated HUVECs were treated with anti-CD109 ABs. The surface of all cellular zones became stiffer after the interaction of HUVECs with anti-CD109 ABs (Figure 4d–f). It is interesting that the stiffening of the nuclear and perinuclear zones is detected to more extent compared to the peripheral zone. For the perinuclear zone, for example, the elastic

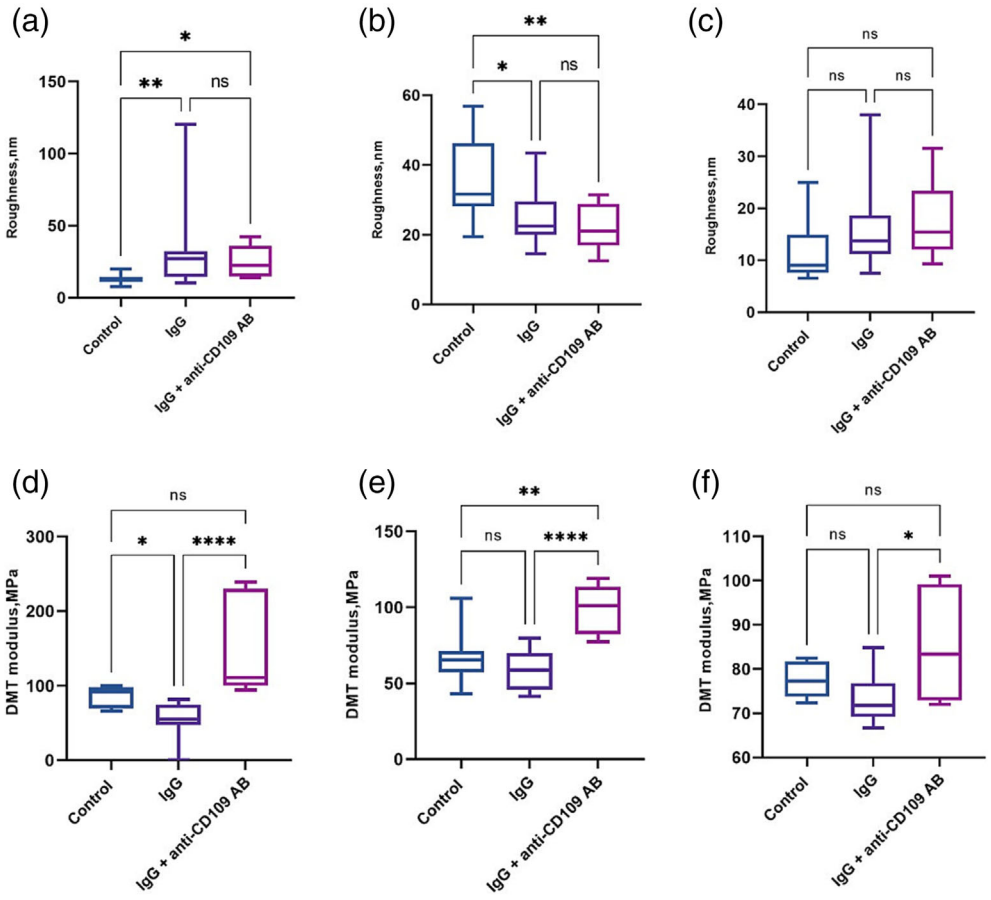

FIGURE 4 Structural and mechanical parameters of fixed HUVEC surface microscale areas for the nuclear (a, d), perinuclear (b, e), and peripheral (c, f) zones. Median roughness of the topographical images (a–c) in nm, median DMT modulus (d–f) in MPa. Data are presented as median, interquartile interval limits (box), and maximal and minimal values (whiskers). Kruskal–Wallis test with Bonferroni correction: $*p < .05$; $**p < .01$; $****p < .0001$; ns $p > .05$.

modulus in 1.45(1.07;2.29) times stiffer than one for control cells and in 2.56(1.90;4.05) times stiffer than one for IgG-treated cells (Me[LQ; UQ], $p < .05$, Mann–Whitney U test).

Figure 5a,b presents the AFM images of the whole living HUVECs of the control sample and the cell sample after the IgG + anti-CD109 AB treatment. Both cell samples are characterized by the presence of well-defined stress fibers (Figure 5c,d). The living cells after the IgG + anti-CD109 AB treatment became in 4.9(3.6;5.9) times stiffer compared to the stiffness of HUVECs of control samples (Me[LQ;UQ], $p < .0001$, Mann–Whitney U test) (Table 1). This difference in the elastic modulus is clearly seen when comparing the profiles of the elastic modulus spatial distribution as shown in Figure 5e.

The results of our deep analysis of the digital complex profiles of the maps of four mechanical parameters (topography, DMT modulus, adhesion, and deformation) using three different classification models of machine learning proved our hypothesis about the significance of the anti-CD109 AB-induced changes in the structural and mechanical parameters of HUVECs (Table A in Appendix S1). The accuracy and effectiveness of classification of the complex profiles of cell surface properties are best observed when using the images of nuclear and perinuclear zones. This result indicates that the maximal changes in the mechanical properties of the HUVECs' surface occur within the nuclei and near nuclei when cells are treated with IgG + anti-CD109 ABs.

4 | DISCUSSION

The interaction of HUVECs with anti-CD109 ABs led to the immobilization of CD109 antigens that supported their removal from the cell pathways, which could result in the TGF-β pathway activation. It is known that all cells perceive TGF-β family signals and elaborate responses affecting cell proliferation, differentiation, communication, adhesion, movement, metabolism, and death (Ma, Sanchez-Duffhues, Goumans, & Ten Dijke, 2020; Melchionna et al., 2021). TGF-β-treatment of cells causes the increase in the sizes of cells (their nuclei and areas of their spreading on a substratum) as shown for NSCLC cells and astrocytes (Gladilin et al., 2019; Moreels, Vandenabeele, Dumont, Robben, & Lambrichts, 2008). Our findings are in agreement with this tendency; after anti-CD109 AB treatment the HUVECs' cell spreading area was increased in comparison with the area after IgG pretreatment.

During the endothelial-to-mesenchymal transition induced by TFG-β molecular and structural changes take place leading to switching between an endothelial to a mesenchymal phenotype. For instance, it results in the loss of characteristic surface endothelial markers, for example, platelet endothelial cell adhesion molecule (PECAM-1/CD31), VE-cadherin, vascular endothelial growth factor receptor (VEGFR), angiopoietin receptor (Tie-2) and the cell–cell junctions (Pardali, Sanchez-Duffhues, Gomez-Puerto, & Ten Dijke, 2017).

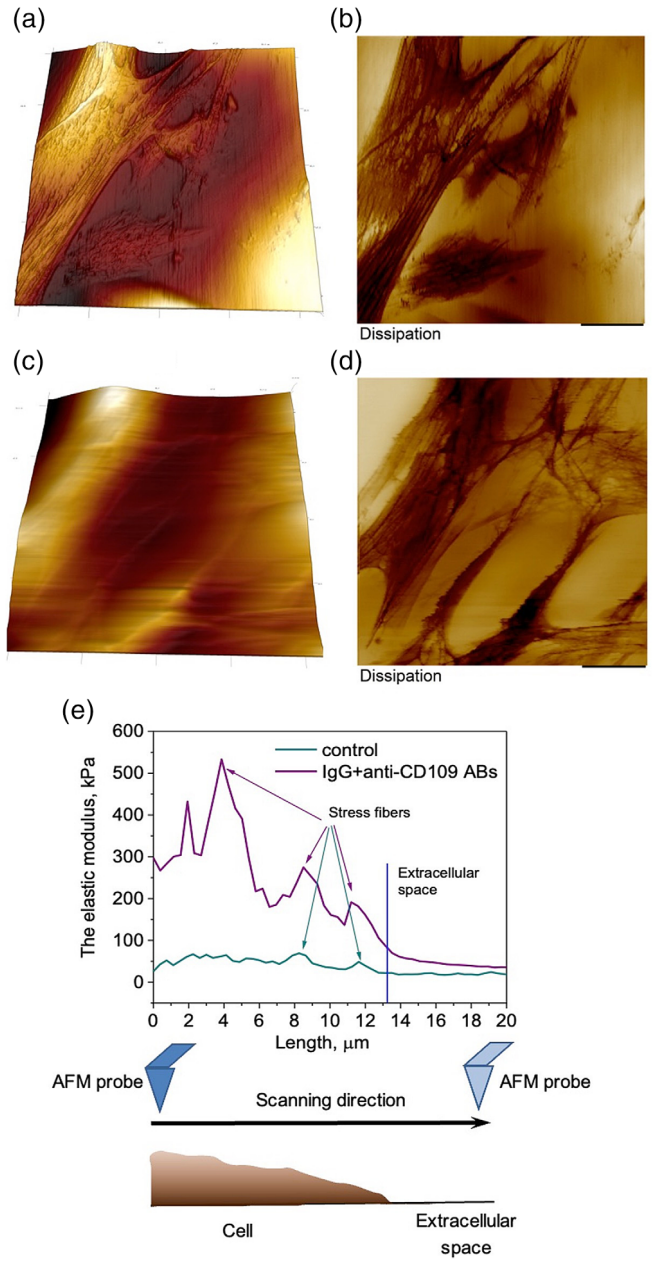

FIGURE 5 Morphology and mechanical parameters of living HUVECs after the IgG + anti-CD109 AB treatment. (a) and (b) AFM images of the whole living HUVECs before the IgG + anti-CD109 ABs treatment (control cells without any treatment). The AFM images were recorded with PeakForce setpoint of 18 pN. (a) 3D topographical image, (b) dissipation map. Scan size is 93.5 μm × 93.5 μm. (c) and (d) AFM images of the whole living HUVECs after the IgG + anti-CD109 ABs treatment. The AFM images were recorded with PeakForce setpoint of 18 pN. The treatment with IgG (15 min) and anti-CD109 ABs (20 min) were performed in the Petri dish after the first scanning (a) and (b). (c) 3D topographical image, (d) dissipation map. Scan size is 94.7 μm × 94.7 μm. (e) The profiles of the DMT modulus of cell samples, recorded as shown in the scheme in the bottom panel. The beginning part of the recorded profile represents a cell, and the remainder of the profile represents the extracellular space (polylysine layer). Cells were recorded in MIROView mode with PeakForce setpoint of 50 pN. The arrows show the peaks of the elastic modulus profiles corresponding to the stress fibers.

TABLE 1 The elastic modulus of cell surface and extracellular surface of control and treated HUVECs' samples.

	DMT modulus, kPa	
Cell sample	**Cell surface**	**Extracellular space**
Control	48.5(32.4;55.8)	11.6(5.5;17.4)
IgG + anti-CD109 ABs	235.0(175.5;283.5)*	19.6(14.9;34.1)

Note: Data are presented as Me(LQ;UQ). Mann–Whitney *U* test:
* $p < .00001$.

Additionally, the switch also results in the gain of characteristic surface mesenchymal markers, for example, α-SMA, smooth muscle 22α (SM22α), fibroblast-specific protein (FSP)-1, fibronectin and vimentin and increase of the cell migratory potential (Pardali et al., 2017).

The TGF-β induces remodeling of the cytoskeleton, both the actin and vimentin structures, that results in an increased cell rigidity (Gladilin et al., 2019). Vimentin filaments form a network that extends from the nuclear periphery towards the plasma membrane of cells of mesenchymal origin including fibroblasts, endothelial cells, and cells of the immune system (Ramos, Stamatakis, Oeste, & Perez-Sala, 2020), and is closely associated with other cytoskeletal components (Battaglia, Delic, Herrmann, & Snider, 2018; Strouhalova et al., 2020). Overexpression of vimentin and some cell adhesion/migration relevant proteins was observed in cells upon epithelial-to-mesenchymal transition or malignant transformation (Lowery, Kuczmarski, Herrmann, & Goldman, 2015). It is known that TGF-β2 induces the formation of cross-linked actin networks which can be completely inhibited by inhibitors of TGF-β receptor, SMAD3, and ERK, as well as completely or partially inhibited by JNK, P38, and ROCK inhibitors, depending on cell strains (Montecchi-Palmer et al., 2017).

Gladilin et al. revealed that the TGF-β-induced cytoskeleton reorganization was not due to the change of G/F-actin ratio but rather crosslinking of the actin cytoskeleton (Gladilin et al., 2019). In our study, the anti-CD109 AB-induced increase in the stiffness of the HUVEC's surface in both the nuclear and perinuclear zones obtained by AFM indicates the formation of a dense structure of the cortical cytoskeleton. The vimentin intermediate filament network formation in those zones was confirmed by the immunocytochemical method. Our data on the elastic modulus of both chemically fixed and living HUVECs support the remodeling of the actin cytoskeleton, which occurs simultaneously with the formation of the vimentin network; since changes in cell stiffness assessed using AFM are mainly associated with rearrangements of the cortical actin cytoskeleton in cells (Starodubtseva, 2022; Starodubtseva et al., 2021).

Recently, the effect of neutralization of CD109 with anti-CD109 ABs has been studied in human fibroblast-like synoviocytes. In that study, cells were stimulated with TNF-α and IL-1β for 12 h, and then subsequently treated with anti-CD109 ABs or IgG for another 24 h. Anti-CD109 AB treatment dose-dependently reduced the levels of IL-6, IL-8, MMP-1, and MMP-3 and the levels of phosphorylated Akt, NF-κB, Stat3, and p38 MAPK irrespective of TNF-α or IL-1β stimulation, as well as reduced cellular migration and invasion (Song

et al., 2019). In our study, the period of observation of anti-CD109 ABs-induced effects in HUVECs was relatively short (45 min). The period within 1 h is generally believed to be too short to affect both transcription and translation, and the changes in cell properties are very likely to be due to alterations in protein modification (especially, protein phosphorylation) (Montecchi-Palmer et al., 2017), suggesting a mechanical role as hypothesized in the study.

From the position of cell biomechanics, one of the obtained results requires high attention. In our previous work, we showed that the mechanical property heterogeneity was inherent for endothelial cells (in the absence of mechanical stress), for example, the perinuclear zone was the softest zone of endothelial cells (Starodubtseva et al., 2021). Here, we revealed that anti-CD109 ABs altered the parameters of the mechanical properties including their spatial distribution on the cell surface. Activation of TGF-β pathways by blocking the CD109 antigen leads to increases in the cell surface stiffness mostly near the nuclei that equalized the difference in the cell mechanical properties among the different cell zones. The inner layer of vessels represents a monolayer of endothelial cells characterized by a specific pattern of mechanical properties influencing the efficiency of the transport of materials from blood to tissue through endothelial cells. The presence of ABs in the blood that potentially influence TGF-β pathways can not only significantly change the averaged mechanical parameters of the endothelial cells but also disturb the pattern of mechanical properties of endothelial cell monolayer that may potentially have a dramatic effect on transcytosis.

Increased stiffness of the cell surface could lead to a high risk of damage to the nucleus-containing compartment of the epithelial cell during pulse pushes. A higher probability of endothelial damage is caused at the sites of blood vessel branching due to turbulent blood flow. In the presence of hyperlipidemia and other risk factors, this creates prerequisites for the emergence and progression of atherosclerosis. A growing number of experimental data confirms that TGF-β-induced endothelial-to-mesenchymal transition is involved in various pathological conditions in adults, including cardiovascular diseases such as atherosclerosis, myocardial infarction, pulmonary hypertension and organ fibrosis (Bischoff, 2019; Zeisberg et al., 2007). The new-established patterns of changes in the mechanical properties of endothelial cells after TGF-β pathway activation leads to a new level of understanding of the development mechanisms of cardiovascular diseases and fibrosis, and provide theoretical justification for the search for promising inhibitors of TGF-β signaling pathways.

The main limitation of the present work is that the present study was carried out using single endothelial cells. In physiology, endothelial cells come into contact with one another, creating a cell monolayer where these cells respond to various factors. The study of the mechanical properties of endothelial cells under the action of anti-CD109 ABs on single cells is the simplest model considering the response of an endothelial cell not taking into account the influence of other cells in a cell monolayer. Further studies will be performed to investigate the effects of anti-CD109 ABs on endothelial cells in monolayer and their functions such as proliferation and migration.

5 | CONCLUSION

In this work, we exclusively studied the mechanical properties and associated changes in HUVECs. For instance, using anti-CD109 antibodies for blocking CD109 antigen of HUVEC's surface we observed cytoskeleton reorganization, increase in averaged stiffness of cell surface, and change in the distribution of cell surface mechanical properties that were accompanied with the activation of the SMAD2/3 proteins, which corresponded to the processes occurring after activation of the TGF-β signaling. CD109-dependent changes in the mechanical properties of endothelial cells could contribute to the development of diseases, including fibrotic diseases and cancer. development of cardiac fibrosis and damage to peripheral vessels are manifested by ischemia and lead to the development of the diseases of the circulatory system, such as ischemic heart diseases, cerebrovascular diseases and diseases of arteries, arterioles and capillaries. Therefore, CD109 antigen may be a potential target and the development of therapeutic methods for the normalization of the impaired TGF-β signaling is a promising area of scientific research.

6 | MATERIALS AND METHODS

6.1 | Cell line and culture conditions

Umbilical cords for the isolation of HUVECs were taken after a successful delivery from an uncomplicated pregnancy. Informed consents to participate in the study were obtained from the subject in labor, and the study protocol was approved by the Ethics Committee of Gomel State Medical University. HUVECs were obtained by flushing the cells after enzymatic treatment of the inner surface of the vessel as described in a recently published report (Starodubtseva et al., 2021). Cells for atomic force microscopy (AFM) analysis were seeded in tissue culture dishes (Cell+, 35 × 10 mm) for adherent cells with an adhesive coating (Sarstedt, Germany) and incubated for 2–4 days under standard cultivation conditions (5% CO_2, 95% humidity, 37°C). For AFM scanning in liquid, the medium in the dishes was replaced with Hanks' Balanced Salt Solution (37°C) (GibcoTM, UK). For AFM scanning in air, the cells were fixed with 2% glutaraldehyde (20 min, 37°C), washed with phosphate-buffered saline, and distilled water and dried at room temperature in a laminar box. HUVECs used were between passages 3 and 6 in all experiments. The purity of isolated HUVEC population was analyzed using an anti-CD31 antibody (Elabscience, China) in immunocytochemistry which revealed >97% positive cells.

6.2 | Cell treatment with antibodies

For blocking Fc-receptors, HUVECs were incubated with IgG (1 μg IgG/10^6 cells, Human IgG Fc antibody/monoclonar mouse IgG_1, clone #97924, R&D Systems) for 15 minutes at room temperature. Then the cells were incubated with anti-CD109 ABs (Human/mouse

CD109 PE-conjugated antibody/monoclonal mouse IgG2A, clone #496929, R&D System, UK) for 30 minutes at room temperature in the dark according to the manufacturer's instructions.

6.3 | Cell staining and light microscopy

Immunocytochemical staining was performed with mouse monoclonal ABs to vimentin (anti-vimentin AB clone V9, Leica Biosystem Newcastle Ltd. [UK]) according to the company's protocol. Novolink Max Polymer Detection System & DAB Chromogen was used as a visualizing system. For the negative control, the samples were incubated with Bond Primary Antibody Diluent (Leica Biosystems Newcastle, Ltd., UK). The relative content of vimentin (N/N_c) in HUVEC samples was assessed relative to the control HUVEC sample. N is the cell area stained in dark brown-violet color (immunocytochemical staining against vimetin) for a studied cell sample. N_c is the median of the cell area stained in dark brown-violet color in cells of the control cell sample. N/N_c is measured in relative units.

For morphological analysis, the fixed cells were stained with Romanovsky-Giemsa solution. The cell samples were analyzed using an Axio Observer 3 microscope, ZenBlue software (Zeiss, UK) and ImageJ software. A parameter of cell spreading area (SA) was used to describe the average contact area of cells with a surface under various experimental conditions and measured using light microscopy images and ImageJ software. SA was estimated based on the analysis in average of 100 cells per experimental sample. Parameter ($100 \times N/N_0$) was used to describe the cell ability to form the filopodia under the different experimental conditions and measured using light microscopic images and ImageJ software. N is the number of cells with filopodia either at the leading edge or on the cell body, N_0 is the total number of cells on a light microscopy image. $100 \times N/N_0$ is measured in percentages.

6.4 | Western blotting

Western blotting was performed as previously described (Cheng et al., 2018). The primary ABs were rabbit anti-Smad2 (1:1000) and rabbit anti-phospho-Smad2 (pSer255) (1:1000) (Abcam, Cambridge, MA), rabbit anti-Smad3 (1:1000), rabbit anti-phospho-Smad3 (pSer423/425) (1:1000) and rabbit anti-GAPDH (Cell Signaling Technology, Beverly, MA) (1:2500). The secondary AB was HRP-conjugated goat anti-rabbit IgG (1:500, Proteintech, Chicago, IL).

6.5 | Atomic force microscopy

In this study, we used Bruker's BioScope Resolve atomic force microscope (AFM) to carry out experiments. Scanning in air was performed using SCANASYST-AIR probes (Bruker, $k = 0.4$ N/m, $R = 2$ nm) in MIROview (PeakForce QNM) mode (NanoScope 9.4 software, Bruker). The surface of the whole cell was scanned using the following parameters: scan size of 100 μm × 100 μm, rate of 0.3 Hz, resolution of 512 × 512 pixels. The small areas of the cell surface were scanned over three typical cell zones: nuclear, perinuclear, and peripheral zones (1 μm × 1 μm, 0.3 Hz, 256 × 256 pixels). Scanning in liquid was performed using PeakForce QNM-Live Cell probes (PFQNM-LC-A-CAL, Bruker, Billerica, MA), short paddle-shaped cantilevers with a pre-calibrated spring constant (0.06–0.08 N/m) and SCANASYST-FLUID probes (Bruker, Billerica, MA) with $k = 0.7$ N/m, $R = 20$ nm in MIROview Live Cells mode at 37°C. Calibration of the probes was performed before scanning the cell samples by contact method according to the protocol of the microscope manufacturer (Bruker PeakForce QNM User Guide, #004-1036-000, 2011). The probe was calibrated at the frequencies of 1 and 0.5 kHz; with a Ramp Size of 300 nm and a Ramp SetPoint of 0.3 V in air, and with a Ramp Size of 300 nm and Ramp Setpoint of 0.2 V in liquid.

6.6 | Data analysis

AFM data analysis was performed using NanoScope Analysis 1.9 software (Bruker) and their statistical analysis of experimental data was performed using OriginPro, version 2019b and Statistical calculator "Statistics Kingdom" (https://www.statskingdom.com/).

The data were checked for compliance with the normal distribution law using the Kolmogorov–Smirnov test. The data are represented as either the median and limits of the interquartile range (Me (LQ; UQ)) or the mean and the limits of 95% confidence interval (95% CI). Multiple comparison analyses were performed using ANOVA Post hoc test (Kruskal–Wallis test with Bonferroni correction) and the comparison between the parameters of two samples was performed using t test or Mann–Whitney U test.

To establish the reliability of significant differences in the structure and mechanical properties of the surface in different areas of the HUVEC surface, the classification of profiles of the cell surface property maps was implemented. We have analyzed the sets of the cell surface AFM images (1 μm × 1 μm, 256 × 256 pixels) recorded in four channels: Adhesion, Height sensor, Log (DMT Modulus), and Deformation. AFM image samples included three "cell treatment" sets (control, IgG-treated cells, and IgG + anti-CD109 AB-treated cells) each of that contained three "cell surface zone" sub-sets (nuclear, perinuclear, and peripheral zones). We carried out the classification of a complex cell surface profile composed of four profiles of different AFM images corresponding to a certain position and containing 1024 (4 × 256) points in each using three algorithms of machine learning: xgboost (implementation of decision trees gradient boosting), k-nearest neighbors, decision trees. Data for each class were randomly divided into training sample (75%) and testing sample (25%). Classification, accuracy estimation, division into training and testing samples, and estimation of the coefficient of determination (R^2) were implemented in Python using the scikit-learn, numpy, pandas, and xgboost libraries.

AUTHOR CONTRIBUTIONS

Maria N. Starodubtseva: Conceptualization, Data curation, Formal analysis, Funding acquisition, Project administration, Supervision, Visualization, Writing- Original draft preparation; Ju Liu: Conceptualization, Funding acquisition, Project administration, Supervision,

Writing-Original draft preparation; Eldar A. Nadyrov: Formal analysis, Validation, Visualization, Writing- Original draft preparation; Nastassia M. Shkliarava: Formal analysis, Investigation, Visualization, Writing-Original draft preparation; Alena U. Sadouskaya: Formal analysis, Investigation, Writing - Original draft preparation; Ivan E. Starodubtsev: Formal analysis, Software; Sergey L. Achinovich: Formal analysis, Investigation, Visualization; Xianli Meng: Investigation, Writing - Original draft preparation; Dmitry A. Zinovkin, Conceptualization, Writing- Reviewing and Editing; Md Zahidul Islam Pranjol: Conceptualization, Funding acquisition, Supervision, Writing - Reviewing and Editing.

ACKNOWLEDGMENTS

The authors thank Aleksey N. Kondrachyk and Matsvei V. Matveyenkau for their kind help in isolation and culturing the HUVEC culture, Marina S. Nedoseikina for her kind help in working with donors and isolation of the umbilical cord.

FUNDING INFORMATION

The work was carried out within the framework of the project of the Belarusian Republican Foundation for Fundamental Research (М20КИ-026, 2020–2021, Belarus) and National.

Natural Science Foundation of China (82011530024).

CONFLICT OF INTEREST STATEMENT

The authors declare no conflict of interests.

DATA AVAILABILITY STATEMENT

The data that support the findings of this study are available from the corresponding author upon reasonable request.

ORCID

Maria N. Starodubtseva https://orcid.org/0000-0002-8516-0884
Md Zahidul Islam Pranjol https://orcid.org/0000-0002-6164-6281

REFERENCES

Battaglia, R. A., Delic, S., Herrmann, H., & Snider, N. T. (2018). Vimentin on the move: New developments in cell migration. *F1000Res*, *7*, 1796. https://doi.org/10.12688/f1000research.15967.1

Beaumont, J., Lopez, B., Hermida, N., Schroen, B., San Jose, G., Heymans, S., … Gonzalez, A. (2014). microRNA-122 down-regulation may play a role in severe myocardial fibrosis in human aortic stenosis through TGF-beta1 up-regulation. *Clinical Science (London, England)*, *126*(7), 497–506. https://doi.org/10.1042/CS20130538

Bischoff, J. (2019). Endothelial-to-mesenchymal transition. *Circulation Research*, *124*(8), 1163–1165. https://doi.org/10.1161/CIRCRESAHA.119.314813

Cheng, Z., Qi, R., Li, L., Liu, Q., Zhang, W., Zhou, X., … Liu, J. (2018). Dihydroartemisinin ameliorates sepsis-induced hyperpermeability of glomerular endothelium via up-regulation of occludin expression. *Biomedicine & Pharmacotherapy*, *99*, 313–318. https://doi.org/10.1016/j.biopha.2018.01.078

Cuppini, L., Calleri, A., Bruzzone, M. G., Prodi, E., Anghileri, E., Pellegatta, S., … Eoli, M. (2013). Prognostic value of CD109+ circulating endothelial cells in recurrent glioblastomas treated with bevacizumab and irinotecan. *PLoS One*, *8*(9), e74345. https://doi.org/10.1371/journal.pone.0074345

de Sousa Lopes, S. M. C., Carvalho, R. L. C., van den Driesche, S., Goumans, M.-J., ten Dijke, P., & Mummery, C. L. (2003). Distribution of phosphorylated Smad2 identifies target tissues of TGFβ ligands in mouse development. *Gene Expression Patterns*, *3*(3), 355–360. https://doi.org/10.1016/s1567-133x(03)00029-2

Frantz, S., Hu, K., Adamek, A., Wolf, J., Sallam, A., Maier, S. K., … Bauersachs, J. (2008). Transforming growth factor beta inhibition increases mortality and left ventricular dilatation after myocardial infarction. *Basic Research in Cardiology*, *103*(5), 485–492. https://doi.org/10.1007/s00395-008-0739-7

Gladilin, E., Ohse, S., Boerries, M., Busch, H., Xu, C., Schneider, M., … Eils, R. (2019). TGFbeta-induced cytoskeletal remodeling mediates elevation of cell stiffness and invasiveness in NSCLC. *Scientific Reports*, *9*(1), 7667. https://doi.org/10.1038/s41598-019-43409-x

Herder, C., Peeters, W., Zierer, A., de Kleijn, D. P., Moll, F. L., Karakas, M., … Koenig, W. (2012). TGF-beta1 content in atherosclerotic plaques, TGF-beta1 serum concentrations and incident coronary events. *European Journal of Clinical Investigation*, *42*(3), 329–337. https://doi.org/10.1111/j.1365-2362.2011.02587.x

Khan, R., & Sheppard, R. (2006). Fibrosis in heart disease: Understanding the role of transforming growth factor-beta in cardiomyopathy, valvular disease and arrhythmia. *Immunology*, *118*(1), 10–24. https://doi.org/10.1111/j.1365-2567.2006.02336.x

Kovacic, J. C., Mercader, N., Torres, M., Boehm, M., & Fuster, V. (2012). Epithelial-to-mesenchymal and endothelial-to-mesenchymal transition. *Circulation*, *125*(14), 1795–1808. https://doi.org/10.1161/circulationaha.111.040352

Kruithof, B. P., Duim, S. N., Moerkamp, A. T., & Goumans, M. J. (2012). TGFbeta and BMP signaling in cardiac cushion formation: Lessons from mice and chicken. *Differentiation*, *84*(1), 89–102. https://doi.org/10.1016/j.diff.2012.04.003

Lee, K. Y., Shueng, P. W., Chou, C. M., Lin, B. X., Lin, M. H., Kuo, D. Y., … Lin, C. W. (2020). Elevation of CD109 promotes metastasis and drug resistance in lung cancer via activation of EGFR-AKT-mTOR signaling. *Cancer Science*, *111*(5), 1652–1662. https://doi.org/10.1111/cas.14373

Lin, M., Sutherland, D. R., Horsfall, W., Totty, N., Yeo, E., Nayar, R., … Schuh, A. C. (2002). Cell surface antigen CD109 is a novel member of the alpha(2) macroglobulin/C3, C4, C5 family of thioester-containing proteins. *Blood*, *99*(5), 1683–1691. https://doi.org/10.1182/blood.v99.5.1683

Lowery, J., Kuczmarski, E. R., Herrmann, H., & Goldman, R. D. (2015). Intermediate filaments play a pivotal role in regulating cell architecture and function. *The Journal of Biological Chemistry*, *290*(28), 17145–17153. https://doi.org/10.1074/jbc.R115.640359

Luckstadt, W., Bub, S., Koudelka, T., Pavlenko, E., Peters, F., Somasundaram, P., … Arnold, P. (2021). Cell surface processing of CD109 by Meprin beta leads to the release of soluble fragments and reduced expression on extracellular vesicles. *Frontiers in Cell and Development Biology*, *9*, 622390. https://doi.org/10.3389/fcell.2021.622390

Ma, J., Sanchez-Duffhues, G., Goumans, M. J., & Ten Dijke, P. (2020). TGF-beta-induced endothelial to mesenchymal transition in disease and tissue engineering. *Frontiers in Cell and Development Biology*, *8*, 260. https://doi.org/10.3389/fcell.2020.00260

Melchionna, R., Trono, P., Tocci, A., & Nistico, P. (2021). Actin cytoskeleton and regulation of TGFbeta signaling: Exploring their links. *Biomolecules*, *11*(2), 336. https://doi.org/10.3390/biom11020336

Mii, S., Enomoto, A., Shiraki, Y., Taki, T., Murakumo, Y., & Takahashi, M. (2019). CD109: A multifunctional GPI-anchored protein with key roles in tumor progression and physiological homeostasis. *Pathology International*, *69*(5), 249–259. https://doi.org/10.1111/pin.12798

Minata, M., Audia, A., Shi, J., Lu, S., Bernstock, J., Pavlyukov, M. S., … Bhat, K. P. (2019). Phenotypic plasticity of invasive edge glioma stem-like cells in response to ionizing radiation. *Cell Reports*, *26*(7), 1893–1905 e1897. https://doi.org/10.1016/j.celrep.2019.01.076

Mo, X. T., Leung, T. H., Tang, H. W., Siu, M. K., Wan, P. K., Chan, K. K., … Ngan, H. Y. (2020). CD109 mediates tumorigenicity and cancer aggressiveness via regulation of EGFR and STAT3 signalling in cervical squamous cell carcinoma. *British Journal of Cancer*, *123*(5), 833–843. https://doi.org/10.1038/s41416-020-0922-7

Montecchi-Palmer, M., Bermudez, J. Y., Webber, H. C., Patel, G. C., Clark, A. F., & Mao, W. (2017). TGFbeta2 Induces the formation of cross-linked Actin networks (CLANs) in human trabecular meshwork cells through the Smad and non-Smad dependent pathways. *Investigative Ophthalmology & Visual Science*, *58*(2), 1288–1295. https://doi.org/10.1167/iovs.16-19672

Moreels, M., Vandenabeele, F., Dumont, D., Robben, J., & Lambrichts, I. (2008). Alpha-smooth muscle Actin (alpha-SMA) and nestin expression in reactive astrocytes in multiple sclerosis lesions: Potential regulatory role of transforming growth factor-beta 1 (TGF-beta1). *Neuropathology and Applied Neurobiology*, *34*(5), 532–546. https://doi.org/10.1111/j.1365-2990.2007.00910.x

Panutsopulos, D., Papalambros, E., Sigala, F., Zafiropoulos, A., Arvanitis, D., & Spandidos, D. (2005). Protein and mRNA expression levels of VEGF-A and TGF-β1 in different types of human coronary atherosclerotic lesions. *International Journal of Molecular Medicine*, *15*(4), 603–610. https://doi.org/10.3892/ijmm.15.4.603

Pardali, E., Sanchez-Duffhues, G., Gomez-Puerto, M. C., & Ten Dijke, P. (2017). TGF-beta-induced endothelial-mesenchymal transition in fibrotic diseases. *International Journal of Molecular Sciences*, *18*(10), 2157. https://doi.org/10.3390/ijms18102157

Ramos, I., Stamatakis, K., Oeste, C. L., & Perez-Sala, D. (2020). Vimentin as a multifaceted player and potential therapeutic target in viral infections. *International Journal of Molecular Sciences*, *21*(13), 4675. https://doi.org/10.3390/ijms21134675

Roopenian, D. C., & Akilesh, S. (2007). FcRn: The neonatal fc receptor comes of age. *Nature Reviews. Immunology*, *7*(9), 715–725. https://doi.org/10.1038/nri2155

Ruwhof, C. (2000). Mechanical stress-induced cardiac hypertrophy: Mechanisms and signal transduction pathways. *Cardiovascular Research*, *47*(1), 23–37. https://doi.org/10.1016/s0008-6363(00)00076-6

Song, G., Feng, T., Zhao, R., Lu, Q., Diao, Y., Guo, Q., … Han, J. (2019). CD109 regulates the inflammatory response and is required for the pathogenesis of rheumatoid arthritis. *Annals of the Rheumatic Diseases*, *78*(12), 1632–1641. https://doi.org/10.1136/annrheumdis-2019-215473

Souders, C. A., Borg, T. K., Banerjee, I., & Baudino, T. A. (2012). Pressure overload induces early morphological changes in the heart. *The American Journal of Pathology*, *181*(4), 1226–1235. https://doi.org/10.1016/j.ajpath.2012.06.015

Starodubtseva, M. N. (2022). Mechanical properties of the cell surface layer measured by contact atomic force microscopy. In F. M. Borodich & X. Jin (Eds.), *Contact problems for soft, biological and bioinspired materials. Biologically-Inspired Systems* (Vol. 15). Springer, Cham. https://doi.org/10.1007/978-3-030-85175-0_3

Starodubtseva, M. N., Nadyrov, E. A., Shkliarava, N. M., Tsukanava, A. U., Starodubtsev, I. E., Kondrachyk, A. N., … Nedoseikina, M. S. (2021). Heterogeneity of nanomechanical properties of the human umbilical vein endothelial cell surface. *Microvascular Research*, *136*, 104168. https://doi.org/10.1016/j.mvr.2021.104168

Strouhalova, K., Přechová, M., Gandalovičová, A., Brábek, J., Gregor, M., & Rosel, D. (2020). Vimentin intermediate filaments as potential target for cancer treatment. *Cancers*, *12*(1), 184. https://doi.org/10.3390/cancers12010184

Sullivan, K. E., & Black, L. D. (2013). The role of cardiac fibroblasts in extracellular matrix-mediated signaling during normal and pathological cardiac development. *Journal of Biomechanical Engineering*, *135*(7), 71001. https://doi.org/10.1115/1.4024349

Tzavlaki, K., & Moustakas, A. (2020). TGF-β signaling. *Biomolecules*, *10*(3), 487. https://doi.org/10.3390/biom10030487

Zeisberg, E. M., Tarnavski, O., Zeisberg, M., Dorfman, A. L., McMullen, J. R., Gustafsson, E., … Kalluri, R. (2007). Endothelial-to-mesenchymal transition contributes to cardiac fibrosis. *Nature Medicine*, *13*(8), 952–961. https://doi.org/10.1038/nm1613

Zhao, Y., Liu, Y., Chen, Z., Korteweg, C., & Gu, J. (2011). Immunoglobulin G (IgG) expression in human umbilical cord endothelial cells. *Journal of Histochemistry and Cytochemistry*, *59*(5), 474–488. https://doi.org/10.1369/0022155411400871

Zhou, S., Cecere, R., & Philip, A. (2017). CD109 released from human bone marrow mesenchymal stem cells attenuates TGF-β-induced epithelial to mesenchymal transition and stemness of squamous cell carcinoma. *Oncotarget*, *8*(56), 95632–95647. https://doi.org/10.18632/oncotarget.21067

Zhou, S., da Silva, S. D., Siegel, P. M., & Philip, A. (2019). CD109 acts as a gatekeeper of the epithelial trait by suppressing epithelial to mesenchymal transition in squamous cell carcinoma cells in vitro. *Scientific Reports*, *9*(1), 16317. https://doi.org/10.1038/s41598-019-50694-z

SUPPORTING INFORMATION

Additional supporting information can be found online in the Supporting Information section at the end of this article.

How to cite this article: Starodubtseva, M. N., Liu, J., Nadyrov, E. A., Shkliarava, N. M., Sadouskaya, A. U., Starodubtsev, I. E., Achinovich, S. L., Meng, X., Zinovkin, D. A., & Pranjol, M. Z. I. (2023). CD109-regulated mechanical properties of endothelial cells. *Cytoskeleton*, *80*(5-6), 123–132. https://doi.org/10.1002/cm.21753